Improved analysis of membrane potential oscillations in the network of cells from islet of Langerhans

Denis Špelič[1], Jurij Dolenšek[2], Andraž Stožer[2,3], Marjan Slak Rupnik[2,3], Borut Žalik[1,3], Domen Mongus[1,3]

1 Faculty of Electrical Engineering and Computer Science, University of Maribor, Smetanova 17, SI-2000 Maribor, Slovenia
2 Institute of Physiology, Faculty of Medicine, University of Maribor, Slomškov trg 15, SI-2000, Maribor, Slovenia
3 Centre for Open Innovations and Research, University of Maribor, Slomškov trg 15, SI-2000, Maribor, Slovenia
{denis.spelic, jurij.dolensek, marjan.rupnik, borut.zalik, domen.mongus}@uni-mb.si; {stozera}@gmail.com

Abstract

This paper proposes a new method for the visualisation of changes in the membrane potentials of biological cells, where the low image resolution and high presence of noise within an original series of images (i.e. a video) prevents accurate observations of this natural phenomenon. This method applies an alpha-trimmed mean filter within time-domain for decomposing a series into high and low frequency bands. Θ-mapping is then applied in order to identify and denoise the signal. Finally, the output images are constructed by suppressing the low-frequency band, whilst high-frequencies are emphasised. As shown by the results, visualisation is significantly improved in this way, whilst the signal-characteristics remain well-preserved.

Keywords: *Scientific visualisation, signal processing, Θ-mapping, islet of Langerhans, beta cell, membrane potential.*

1. INTRODUCTION

Islets of Langerhans are comprised of beta cells that secrete the anabolic hormone insulin [5]. Insulin is secreted into the circulation interprandially (i.e. between meals), keeping at bay the catabolism of bodily energy reserves, as well as postprandially (i.e. after meals) when the concentration of nutrients in the plasma increases, thus enabling the storage of energy-rich molecules in the forms of liver and muscle glycogen as well as fat-tissue triglycerides, and promoting protein anabolism [18]. The absence of insulin due to the destruction of islets but also a partial lack of its effects due to the resistance of tissues to insulin or a decreased secretion of insulin all result in a severe and chronically disabling clinical picture known as diabetes mellitus [2]. The global prevalence of diabetes mellitus in people aged 20-79 years was 8.3 % in 2011, consuming on average 11% of national healthcare budgets. However, the global prevalence in this age group is expected to increase by 50 % by 2030, thus presenting in depth motivation for researchers and their funders [19].

Islets present 1-2 % of the pancreas in mass and volume. They have a spherical structure (100-300 μm in diameter) and are comprised of a few thousand cells per islet [6]. Glucose-responsive and insulin-secreting cells named beta cells comprise the highest fraction of the cells inside the islets of Langerhans [7]. The cells are functionally coupled via connexin36 molecules forming a syncytium of cells [15]. Due to the current consensus model, glucose and other nutrients enter the beta cell, are then metabolised yielding ATP that decreases the open probability of a specific channel protein conducting K^+ in an ATP-dependent manner (K_{ATP} channels) and depolarises the cell membrane [1,4]. Following the initial depolarisation, the membrane potential (MP) in the cells oscillates in the form of bursts with superimposed high frequency spikes. Tightly-coupled with the bursts is the change in the intracellular concentration of Ca^{2+} ($[Ca^{2+}]_i$), oscillating phase-locked to the MP signal. The dynamics and network properties of the $[Ca^{2+}]_i$ signal within a large number of simultaneously studied beta cells have been described recently [16,17]. Each oscillation originating in a single (or possibly a few) cell(s) spreads in a wave-like pattern throughout the islet [16]. The extent and exact nature of coupling the MP signal to the wave of the $[Ca^{2+}]_i$ oscillation is presently unknown; the main reason being that when using the state-of-the-art electrophysiological approach, changes in MP can only be collected for a single or at most two cells from the networks of active beta cells [8]. In contrast, laser-scanning confocal $[Ca^{2+}]_i$ imaging has been shown to provide data for many cells inside the beta cell network, with impeccable temporal and spatial resolutions [16]. To date, to the best of our knowledge, no reports have succeeded in using voltage-sensitive dyes to assess the electrical activities within networks of beta cells.

Recently, a novel family of voltage-sensitive dyes called VoltageFluor (VF) was introduced [9]. The dye incorporates within the outer leaflet of the cell membrane and its fluorescence changes by 2-3% for every 10 mV change in MP. The VF displays a several-fold increased voltage-sensitivity compared to the older families of voltage-sensitive dyes. We loaded islets of Langerhans in acute pancreatic tissue slices with the VF dye and stimulated them with 12 mM glucose, the most important nutrient secretagogue for beta cell activation. The VF signal during the glucose stimulation is comprised of rhythmical increases in fluorescence, most probably reflecting the characteristic oscillatory changes in MP recorded using a patch pipette. The MP signal spreads over the islets in a manner similar to the one observed for $[Ca^{2+}]_i$ waves, with comparable durations of oscillations and velocities of wave-fronts. In order to resolve the degree of coupling between the MP and $[Ca^{2+}]_i$ signals, double staining with voltage- and calcium-sensitive dyes is needed or, alternatively, a stimulus that would enable the detecting of differences between the two signals. Adding tetraethylammonium (TEA, 10 mM), a potent K^+ channel inhibitor, to extracellular solution already containing a stimulatory concentration of glucose (12 mM), is expected to increase the size of the MP oscillations whilst shortening them at the same time [3]. Both effects can help unmask any potential temporal differences in the MP vs. $[Ca^{2+}]_i$ kinetics masked by the longer oscillation durations during the glucose-only stimulation. Unfortunately, in addition to its benefits, TEA stimulation presents technical complications due to a faster spreading of the wave (1000 μm/s) and relatively short oscillation duration (100 ms). In order to achieve a sufficiently high temporal resolution, (i) a decrease in spatial resolution or (ii) a worsening of the signal-to-noise ratios of the single frames is needed (see example in Fig. 1a). Both results demand improved analysis of the MP wave spatiotemporal images.

Unfortunately, the obtained images are highly noisy and only experts can interpret them correctly. In order to cope with high noise and low image resolution, we employed an approach based on connected operators of mathematical morphology [14]. Namely, by acting on connected pixels with constant intensities (called flat-zones) rather than individual pixels, the connected operators uphold good contour preservation properties and are able to prevent significant image distortions when applied for filtering. Section 2 provides definitions of the connected operators used in this paper. The new approach for image filtering is proposed in Section 3. The results are shown in Section 4, whilst Section 5 concludes the paper.

2. THEORETICAL BACKGROUND

Let $f: E \to \mathbb{N}$, where $E \subset \mathbb{N}^2$, be an image, $p \in E$ a pixel, and $T_l = \{p \mid f[p] > l\}$ a threshold set of f obtained at level l. A peak connected-component $C_l^p \in T_l$ is a connected set of pixels from T_l containing p, whilst the relationship $l' \geq l \to T_{l'} \subseteq T_l$ explains the nesting of peak connected-components. An attribute opening $\gamma_a^A(f)$ acting on f is an operator that removes all C_l^p with an attribute value $A(C_l^p)$ smaller than a given threshold a. Note that increasing attributes are described by the relationship $C_{l'}^p \subseteq C_l^p \to A(C_{l'}^p) \leq A(C_l^p)$ and further definitions are given only for them. Examples of such attributes are the area of C_l^p, its volume or its diagonal. An attribute closing, denoted as ϕ_a^A, is a dual operator of γ_a^A and it is given by $\gamma_a^A(f) = -\phi_a^A(-f)$ [10]. An image decomposition, named differential attribute profiles (DAP), that is based on granulometries of attributed openings was proposed by Ouzounis et al. [12]. A granulometry is an ordered set of morphological filters that progressively reduce the content of the image by filtering it on an increasing scale. A glanulometry based on the attribute *A* with *N+1* members is defined by a set of attribute threshold values $\boldsymbol{a} = \{a_i\}$, where $a_{i-1} < a_i$ and $i \in [0, N]$. The definition of DAP obtained from *f*, is given as

$$\Gamma_{\boldsymbol{a}}^A(f) = \left\{\gamma_{a_{i-1}}^A(f) - \gamma_{a_i}^A(f)\right\}, \qquad (1)$$

where $i \in [1, N]$. Thus, DAP is a top-hat scale-space obtained from *f*, where $\Gamma_a^A(f)[p]$ is a vector containing *N* response values obtained at *p*. This vector is named the positive response vector whilst it's dual (i.e. negative response vector) is obtained by an ordered set of attribute closings, and is denoted as $\Phi_a^A(f)$.

Recently, Mongus and Žalik [10] proposed extraction of the most-contrasted connected-components from $\Gamma_{\boldsymbol{a}}^A(f)$ by a mapping schema named Θ-mapping. Consider a set of peak connected-components $C^p = \{C_l^p\}$ containing p. The most-contrasted connected-component $C_{max}^p \in C^p$ with respect to the given $\Gamma_{\boldsymbol{a}}^A(f)$ can be uniquely identified by registering the largest response contained in $\Gamma_{\boldsymbol{a}}^A(f)[p]$ and the associated attribute threshold value at which it was obtained. Θ-mapping is, therefore, given by $\Theta_{\boldsymbol{a}}^A: f \to (R(f), Q(f), P(f))$, where

- $R(f)$ is a transformation function registering maximal responses obtained at pixel p and is formally given by
$$R(f)[p] = max\ \Gamma_{\boldsymbol{a}}^A(f)\,[p]. \qquad (2)$$
- $Q(f)$, called associated function, maps the attribute value that lead to the maximal response. Formally it can be written formally as
$$Q(f)[p] = max\, i \mid \Gamma_{\boldsymbol{a}}^A(f)\,[p][i] = R(f)[p]. \qquad (3)$$
Note that due to the increasing property of A, there exist at most one C_l^p where $A(C_l^p) = Q(f)[p]$ and thus it defines C_{max}^p. However, it is possible that no response is obtained at a given p, meaning that the corresponding peak connected-components are not in contrast against their surroundings in regard to the given $\Gamma_{\boldsymbol{a}}^A(f)$. In this case, p is recognised as a background [10].
- $P(f)$ is an arbitrary parameter that can be measured for C_{max}^p and can be used for estimating multiple characteristics that lead to a particular response. Formally, it can be defined as
$$P(f)[p] = parameter(C_{max}^p). \qquad (4)$$

3. REMOVAL OF NOISE FROM LOW RESOLUTION IMAGES OF BIOLOGICAL CELLS

This section proposes a new method for the improved monitoring of membrane-potential oscillations in a time-series data (i.e. a video). This method consists of the following three steps:

- Firstly, detection of changes is achieved by decomposing images from the time-series into a series of high-frequency differences and low-frequency alpha-trimmed mean images.
- Θ-mapping is then applied on each high-frequency image in order to detect and remove noise.
- Finally, output images are constructed by adding the filtered images of differences to the low-frequency images.

In the continuation, these three steps are explained in detail.

3.1 Image smoothing

The first step of the proposed method considers smoothing within the time-domain in order to obtain a representative image of the cells' structures and, consequentially, identify potential candidates for the noise pixels. Since no changes are expected in the positions of the cells over a short period of time, changes between the successive images can be related to the changes in the membrane potential and the presence of noise. Smoothing the images through the time-domain should, therefore, allow for efficient estimation of the image's structural part, whilst the textural part (i.e. the image of differences between the original and smoothed image) should contain most of the noise. It can, furthermore, be claimed that short, high-contrasted changes (e.g. high increases or decreases of intensity) are most-probably introduced by the impulse noise. This, consequentially, leads to applying a band-pass alpha-trimmed mean filter to each pixel within the time-domain. Let a time-series $f = \{f_t\}$, where $t \in [0, T]$, and a function $\max^{(n)}\{f_t[p]\}$ estimate the nth largest value contained in the set of values $\{f_t[p]\}$. The alpha-trimmed mean filter $\Lambda_\alpha^w(f_t)$ acting on f_t with a window size w is at a pixel p given by [13]

$$\Lambda_\alpha^w(f_t)[p] = \frac{1}{1+2(w-\alpha)} \sum_{n=\alpha}^{2w+1-\alpha} \max^{(n)}\{f_{t'}[p]\}, \qquad (5)$$

where $t' \in [t-w, t+w]$, and α defines the number of trimmed values. Each f_t is then decomposed into a high-frequency f_t^S (structural) and low-frequency f_t^T (textural) part, where $f_t^S = \Lambda_{10}^{50}(f_t)$ and $f_t^T = \Lambda_1^2(f_t - f_t^S)$. Note that trimming values α (and consequentially w) were defined according to the oscillations in the average image intensity (see Figure 1). Namely, $\alpha = 1$ was selected when constructing f_t^T since no significant oscillations can be noticed over such a short period of time. On the other hand, $\alpha = 10$ was selected when constructing f_t^S since all the oscillations are up to 10 frames long. In this way, we ensure that the signal is entirely contained in f_t^T, that is further processed. The obtained f_t^S and f_t^T are shown in Fig. 1.

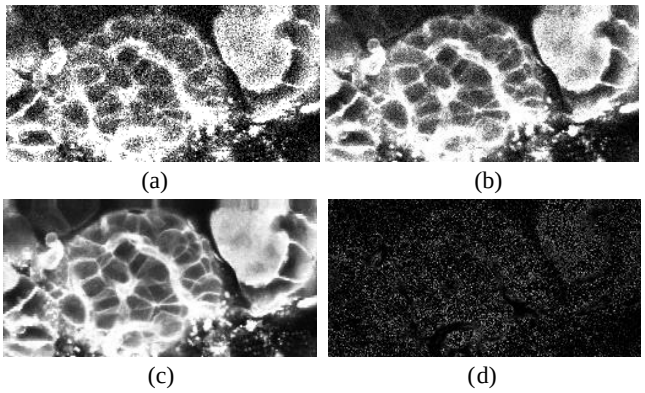

Figure 1: Input frame 55 (a) filtered with w=5, $\boldsymbol{\alpha} = \mathbf{1}$ (b), filtered with w=50, $\boldsymbol{\alpha} = \mathbf{10}$, and the obtained $\boldsymbol{f_t^S}$ (c) and $\boldsymbol{f_t^T}$ (d).

3.2 Noise filtering

Although the alpha-trimmed averaging performed in the previous step sufficiently reduced the impulse noise from the original series of images, it does not remove the noise that is present for more than a single frame. Additional filtering is, therefore, performed within the space-domain of the textural image f_t^T. In this case, noise may be described as a set of small compact regions with high contrast against their surroundings. Thus, Θ-mapping provides an efficient approach for its identification. For this purpose, the definition of the underlying DAP is considered first.

In order to avoid relying on any particular shape when estimating the most-contrasted connected-components, area attribute A was used and the same area threshold vector $\boldsymbol{a}$ is defined for all f_t^T. Due to the low image resolution, sufficient results were obtained using relatively small area-zones defined as $\boldsymbol{a} = \{3 * i\}$, where $i \in [0,10]$. The shape-compactness parameter of the most-contrasted connected-component was then estimated by Θ-mapping using shape-based filtering support. Thus, the value of $P(f_t^T)$ at a particular pixel p is defined as [11]

$$P(f_t^T)[p] = \frac{A(C_{max}^p)}{9\pi * \overline{DT}(C_{max}^p)}, \quad (6)$$

where $A(C_{max}^p)$ is the area of C_{max}^p and $\overline{DT}(C_{max}^p)$ is the average value of the well-known distance transformation performed on C_{max}^p. A set of noise pixels p^* is then defined by

$$p^* = \{p \mid R(f_t^T)[p] > 10.0, P(f_t^T)[p] < 10.0\}, \quad (7)$$

where the threshold values were defined according to the amplitudes of the oscillations in the average intensity graph (see Figure 1). Finally, the same filtering principle was performed for the removal of the dark noise by applying Θ-mapping on the negative response vector (obtained by an ordered set of area closings $\Phi_a^A(f)$).

3.3 Image reconstruction

In the last step of the method, textural images f_t^T are denoised first and then added to the structural images f_t^S in order to obtain a filtered version of the original time-series f'. First, the filtered textural image $f_t^{T\prime}$ is obtained by

$$f_t^{T\prime}[p] = \begin{cases} f_t^T[p]; & p \notin p^* \\ f_t^T[p] - R(f_t^T)[p]; & p \in p^* \end{cases}. \quad (8)$$

A convolution with a 3×3 Gaussian kernel is then performed on $f_t^{T\prime}$ in order to smooth out any possible irregularities introduced by eq. 10 and the output can finally be given as $f'_t = f_t^S + f_t^{T\prime}$.

4. RESULTS

The proposed method is compared with the existing approach for the detection of changes in membrane potential, where a region of interest (ROI) is selected in order to monitor changes in the average intensity (see Fig. 2). Although averaging improves the resistance of the method against noise, it does not remove it (i.e. in Fig. 2c only the middle peak represents actual signal). However, this approach does not allow monitoring a single pixel.

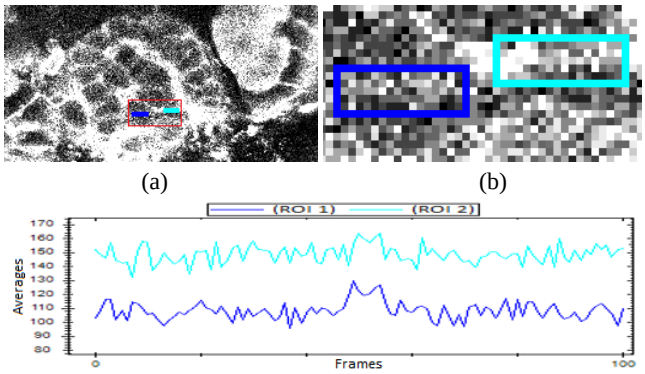

Figure 2: Input frame 55 with ROIs (a) magnification of region containing ROIs (b) and corresponding chart of average values within selected ROIs (c).

In figure 2a, frame 55 from the input video is shown with two selected ROIs (magnification in Fig. 2b). The corresponding time series of average intensities are shown in Fig 2c. A significant change in the membrane potential can be recognised between frames 45 and 55, as it is similar in both regions, whilst significant differences in oscillations can be observed outside of this range. These are characteristics should, therefore, be preserved by the proposed method, whilst visualisation of the signal propagation should be enhanced.

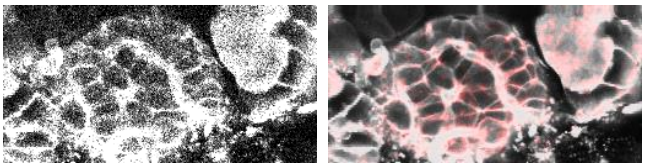

Figure 3: Input frames 55 (a), enhanced after noise filtering (b).

The results of the method are shown in Fig. 3, where frame 55 is used for the comparison. Significant denoising can be observed, whilst visualising the signal in the red channel emphasises the representations of changes for improved analysis.

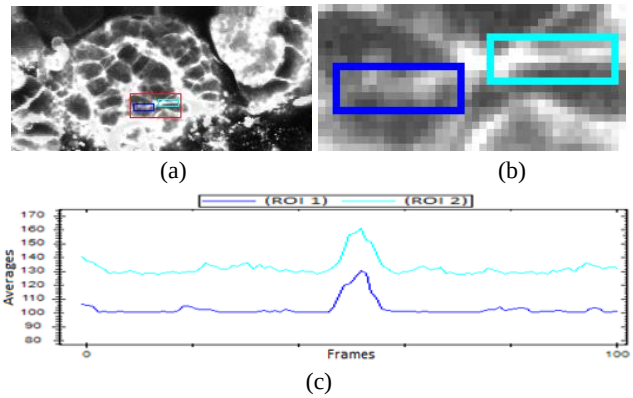

Figure 4: Output frame 55 (a) with ROIs (b) and corresponding chart of average values within selected ROIs (c).

Finally, the method has been evaluated in terms of monitoring the average intensity in ROIs. An important improvement achieved by the proposed method can be observed in Fig. 4. Fig. 4a shows output frame 55 where significant de-noise has been achieved and the magnifications of those area containing selected ROIs are shown in Fig. 4b. By comparing the obtained time-series charts (Fig. 4c) with the original (Fig. 2c), a significant noise reduction can also be observed in this case, whilst even the actual impulse in the membrane potential has been emphasised. Consequentially, further analysis can significantly be improved.

5. CONCLUSION

This paper proposed an improved method for monitoring changes in the membrane potentials of biological cells. This method is able to remove the impulse noise by alpha-trimmed mean filtering applied on a series of images within the time-domain. The derived band-pass filter, moreover, allows for accurate extraction of the actual signal, while mapping has proved to be an efficient tool for the detection of noise within the space-domain. By using this extraction of the signal in a separate band, improved visualisation can be achieved, where the signal can be enhanced and mapped into different coloured channels (e.g. red). Future work will consider an analysis of the time-series charts of average intensities for an automatic definition of the used threshold values.

6. ACKNOWLEDGEMENTS

This work was supported by the Slovenian Research Agency under grants P2 – 0041 and through Centre of Excellence for Integrated Approaches in Chemistry and Biology of Proteins. Present paper was produced within the framework of the operation entitled “Centre for Open Innovation and Research of the University of Maribor”. The operation is cofounded by the European Regional Development Fund and conducted within the framework of the Operational Programme for Strengthening Regional Development Potentials for the period 2007 – 2013, development priority 1: “Competitiveness of companies and research excellence”, priority axis 1.1: “Encouraging competitive potential of enterprises and research excellence".

7. REFERENCES

[1] Ashcroft FM, Harrison DE, Ashcroft SJ (1984) Glucose induces closure of single potassium channels in isolated rat pancreatic beta-cells. Nature 312: 446-448.

[2] Association AD (2012) Diagnosis and Classification of Diabetes Mellitus. Diabetes Care 35: S64-S71.

[3] Atwater I, Ribalet B, Rojas E (1979) Mouse pancreatic beta-cells: tetraethylammonium blockage of the potassium permeability increase induced by depolarization. The Journal of Physiology 288: 561-574.

[4] Dean PM, Matthews EK (1968) Electrical Activity in Pancreatic Islet Cells. Nature 219: 389-390.

[5] Henderson JR (1969) WHY ARE THE ISLETS OF LANGERHANS? The Lancet 294: 469-470.

[6] Hellman B (1959) Actual distribution of the number and volume of the islets of Langerhans in different size classes in non-diabetic humans of varying ages. Nature 184(19): 1498-1499.

[7] Kim A, Miller K, Jo J, Kilimnik G, Wojcik P, et al. (2009) Islet architecture: A comparative study. Islets 1: 129-136.

[8] Meissner HP (1976) Electrophysiological evidence for coupling between [beta] cells of pancreatic islets. Nature 262: 502-504.

[9] Miller EW, Lin JY, Frady EP, Steinbach PA, Kristan WB, Jr., et al. (2012) Optically monitoring voltage in neurons by photo-induced electron transfer through molecular wires. Proceedings of the National Academy of Sciences of the United States of America 109: 2114-2119.

[10] Mongus D and Žalik B (2013) Computationally efficient method for the generation of a digital terrain model from airborne LiDAR data using connected operators IEEE J of Selected Topics in Applied Earth Observations and Remote Sensing in press.

[11] Montero RS and Bribiesca E (2009) State of the art of compactness and circularity measures. In International Mathematical Forum 4(25-28): 1305-1335.

[12] Ouzounis GK, Pesaresi M, and Soille P (2012) Differential area profiles: Decomposition properties and efficient computation. IEEE Transactions on Pattern Analysis and Machine Intelligence 32(8): 1533–1548.

[13] Oten R and Figueiredo RJ (2004) Adaptive alpha-trimmed mean filters under deviations from assumed noise model. IEEE Transactions on Image Processing 13(5): 627-639.

[14] Salembier P and Wilkinson MHF (2009) Connected operators: A review of region-based morphological image processing techniques. IEEE Signal Processing Magazine 136(6): 136–157.

[15] Serre-Beinier V, Le Gurun S, Belluardo N, Trovato-Salinaro A, Charollais A, et al. (2000) Cx36 preferentially connects beta-cells within pancreatic islets. Diabetes 49: 727-734.

[16] Stožer A, Dolenšek J, Rupnik MS (2013) Glucose-Stimulated Calcium Dynamics in Islets of Langerhans in Acute Mouse Pancreas Tissue Slices. PLoS ONE 8: e54638.

[17] Stožer A, Gosak M, Dolenšek J, Perc M, Marhl M, et al. (2013) Functional Connectivity in Islets of Langerhans from Mouse Pancreas Tissue Slices. PLoS Comput Biol 9: e1002923.

[18] Taylor SI (1999) Deconstructing Type 2 Diabetes. Cell 97: 9-12.

[19] Unwin N, Whiting D, Gan D, Jacqmain O, Ghyoot G (2012) IDF Diabetes Atlas. Brussels: International Diabetes Federation, p. 143.

About the author

Denis Špelič is an assistant researcher at Faculty of Electrical Engineering and Computer Science at University of Maribor.

Jurij Dolenšek is an assistant researcher at Faculty of Medicine at University of Maribor.

Andraž Stožer is an assistant researcher at Faculty of Medicine at University of Maribor.

Marjan Slak Rupnik is a professor at Faculty of Medicine at University of Maribor.

Borut Žalik is a professor at Faculty of Electrical Engineering and Computer Science at University of Maribor.

Domen Mongus is an assistant professor at Faculty of Electrical Engineering and Computer Science at University of Maribor.